

Time Delay Margin Analysis
for Adaptive Flight Control Laws

A THESIS
SUBMITTED TO THE FACULTY OF THE GRADUATE SCHOOL
OF THE UNIVERSITY OF MINNESOTA
BY

Andrei Dorobantu

IN PARTIAL FULFILLMENT OF THE REQUIREMENTS
FOR THE DEGREE OF
MASTER OF SCIENCE

Peter J. Seiler, co-advisor
Gary J. Balas, co-advisor

December 2010

© Andrei Dorobantu 2010

Acknowledgments

I want to thank all those around me who supported me through the years. It has been a long journey that was crazy at times. I would never have been able to get any research together without your constant encouragement and cheer. For that I want to say thanks to my parents, my brother, Joe, and everyone else in lab 15 for dealing with me.

I also want to single out and thank Pete Seiler for his countless hours devoted to helping me iron out little odds and ends. I hope to one day explain to you something going on “under the hood”.

Finally, none of this would have been possible without the guidance of my advisor Gary Balas. I have come a long way since undergrad thanks to you. No matter what, I will always remember to step back and first consider the results of the linear analysis.

This research was partially supported under the NASA Langley NRA contract NNH077ZEA001N entitled “Analytical Validation Tools for Safety Critical Systems” and the NASA Langley NRA Contract NNX08AC65A entitled “Fault Diagnosis, Prognosis and Reliable Flight Envelope Assessment.” I would like to thank the technical contract monitors Dr. Christine Belcastro and Dr. Suresh Joshi, respectively.

Dedication

To My Family and Joe

Abstract

Adaptive control algorithms have the potential to improve performance and reliability in flight control systems. Implementation of adaptive control on commercial and military aircraft requires validation and verification of the control system robustness to modeling error and uncertainty. Currently, there is a lack of tools available to rigorously analyze the performance and robustness of adaptive systems due to their inherently nonlinear dynamics. This thesis addresses the development of nonlinear robustness analysis tools for adaptive flight control systems. First, a model reference adaptive controller is derived for an aircraft short period model. It is noted that the controller is a polynomial system. Polynomial optimization tools are then applied to the closed-loop model to assess its robustness to time delays. Time delay margins are computed for various tuning of design parameters in the adaptive law, as well as in the presence of model uncertainty.

Contents

List of Figures	vi
Chapter 1 Introduction	1
Chapter 2 Aircraft Dynamics and Adaptive Control	3
2.1 Short Period Aircraft Dynamics	4
2.2 Model Reference Adaptive Control	6
2.3 Key Properties of the Closed-Loop System	9
Chapter 3 Sum-of-Squares Optimization	13
Chapter 4 Stability Analysis	16
4.1 Global Stability Conditions	16
4.2 Local Sum-of-Squares Stability Conditions	20
Chapter 5 Problem Formulation	24
Chapter 6 Results	30
6.1 Adaptation Rate	32
6.2 Sigma Modification	36

6.3 Aircraft Model Uncertainty	39
6.4 Limitations	43
Chapter 7 Conclusion	44
Bibliography	46

List of Figures

2.1 System interconnection for aircraft model with MRAC.	6
4.1 Graphical interpretation of S-procedure constraint relaxation.	21
5.1 System interconnection for time delayed aircraft model with MRAC.	25
5.2 Simplified system interconnection neglecting input reference signal.	26
5.3 Randomly selected initial condition trajectories.	27
5.4 Level sets of Lyapunov function and box in state space.	28
6.1 Bode plot of open-loop aircraft model and inner-loop.	31
6.2 Finding minimum influential adaptation rate: $\kappa = [0, 0.5]$	33
6.3 Trend in response due to increasing adaptation rate: $\kappa = [0.5, 1, 2, 5]$	33
6.4 Trend in response due to increasing adaptation rate: $\kappa = [5, 100, 500]$	34
6.5 Time delay margin bounds as functions of adaptation rate.	35
6.6 Finding maximum sigma modification value: $\sigma = [0, 2]$	37
6.7 Time delay margin bounds as functions of sigma modification.	38
6.8 Bode plot illustrating aircraft model uncertainty.	40
6.9 Root locus due to aircraft model uncertainty.	41
6.10 Time delay margin bounds as functions of aircraft model uncertainty.	42

Nomenclature

Abbreviations and Acronyms

<i>MRAC</i>	Model Reference Adaptive Control
<i>SOS</i>	Sum-of-Squares
<i>SDP</i>	Semidefinite Programming

List of Symbols

t	Time, <i>sec</i>
α	Angle-of-Attack, <i>rad</i>
q	Pitch Rate, <i>rad/s</i>
r	Time Delay, <i>sec</i>
τ	Time Delay Interval, <i>sec</i>
x	Aircraft State Vector
θ	Adaptation Parameter State Vector
λ_α	Angle-of-Attack Uncertainty Scaling
λ_q	Pitch Rate Uncertainty Scaling
P_λ	Uncertain Longitudinal Aircraft Dynamics Model
A_{nom}	Nominal Aircraft Dynamics State Matrix
K_x	Full State Feedback Term
K_r	Reference Feedforward Term
V	Lyapunov Function
\dot{V}	Lyapunov Function Time Derivative

Chapter 1

Introduction

Adaptive control laws show great potential to improve the performance and reliability of flight control systems. Adaptive control laws are typically nonlinear and time-varying. Generally, few tools exist to rigorously analyze the robustness and performance of such systems. The lack of tools available to verify performance and robustness is a significant roadblock to the implementation of adaptive controllers on military and civilian aircraft.

The objective of this thesis is to demonstrate the suitability of sum-of-squares polynomial optimizations for the analysis of adaptive flight control systems. There has recently been significant research on sum-of-squares optimization problems [1-3]. These optimization problems involve constraints on polynomial functions and can be used to analyze the performance and robustness of systems described by polynomial dynamics. Computational algorithms have been developed for estimating regions of attraction, reachability sets, input-output gains, robustness with respect to uncertainty, and time delay margins [4-20]. Moreover, there is freely available software to solve sum-of-squares optimizations, which allows for easy application of these techniques to aerospace systems [21-23].

This thesis demonstrates that sum-of-squares optimization tools can be applied to assess the robustness of adaptive flight control laws. The approach has been previously applied to simple one-state model reference adaptive control systems [17,24]. In this thesis, a more insightful aircraft model is considered for model reference adaptive control.

An important and meaningful robustness metric for the analysis of adaptive flight control systems is the time delay margin. The sum-of-squares approach is used to calculate lower bounds on this robustness metric. The analysis in this thesis focuses on a realistic flight control problem and the engineering insight that can be drawn from the nonlinear analysis.

The following structure outlines the flow of the thesis. In Chapter 2, a model reference adaptive controller is defined for the linear short period dynamics of an aircraft. It is noted that this controller is a polynomial system, hence the full closed-loop system can be modeled as a polynomial dynamical system. Sum-of-squares optimization tools are ideally suited to analyze the robustness of such systems because they are governed by polynomial dynamics. Chapter 3 provides a brief theoretical background description of sum-of-squares optimizations. An overview of the freely available analysis tools related to the optimizations is also included. Chapter 4 derives a set of sum-of-squares conditions for calculating lower bounds on the time delay margin. Chapter 5 properly formulates a time delayed version of the closed-loop model reference adaptive control system as a sum-of-squares optimization problem. Chapter 6 summarizes the findings from the analysis. Chapter 7 serves as a wrap-up and conclusion for the thesis.

Chapter 2

Aircraft Dynamics and Adaptive Control

Simple linear dynamical systems are convenient from an analysis and computational perspective. However, real engineering systems are frequently complicated and nonlinear. A useful mathematical model must sufficiently emulate the real system for the results to be applicable, but also retain computational tractability. Implementing the right quantity of model complexity is crucial towards obtaining meaningful results from analysis.

Aircraft systems are governed by highly coupled and nonlinear dynamics. The longitudinal flight dynamics can be decoupled from the rest, which is very useful for model simplification. Under normal flight conditions, i.e. when the aircraft is not stalled, linearized longitudinal dynamics accurately predict the behavior of the real system. Therefore, linear dynamics comprise a reasonable abstraction of the true aircraft in this case. The dynamics can be further broken into two modes, each with a drastically different time scale. The faster of the two is usually referred to as the short period. The short period dynamics overwhelmingly dominate the aircraft response relevant to handling and control in the longitudinal axis [25]. Hence, these linear dynamics are suitable for the focus of analysis because they are simple, yet closely approximate the behavior of the real system.

Adaptive control is attractive because it has potential to improve the reliability of aircraft control systems. Generally, it provides an efficient and automatic way to

handle modeling uncertainty. A multitude of adaptive control architectures have been proposed over the past decades. Most include nonlinear components in their control law definitions. A well-studied such example is model reference adaptive control (MRAC). Applying MRAC to aircraft short period dynamics forms a relatively simple model with nonlinear characteristics. This model is useful for developing nonlinear analysis tools needed for validating the robustness of adaptive control laws.

2.1 Short Period Aircraft Dynamics

The longitudinal dynamics for conventional aircraft can be linearized about equilibrium flight conditions, commonly referred to as trim conditions. From a trim condition, small perturbations result in linear responses from the system. Altitude is a component of the longitudinal axis dynamics, but is neglected in this analysis. Assuming level flight, altitude variations are small and have a negligible effect on the aircraft. Altitude enters the equations of motion through changes in the static air pressure, which are insignificant when considering small perturbations from trim.

The resulting linear system is fully described by four states: angle-of-attack, pitch rate, pitch angle, and velocity. Eigenvalue decomposition of the corresponding state matrix reveals that the longitudinal dynamics are governed by two oscillatory modes: the phugoid and the short period. The phugoid is a lightly damped mode with a long period of oscillation, on the order of 0.1 rad/sec. It dominates the pitch angle and velocity state responses. The short period is also lightly damped but, as its name implies, has a quicker transient, on the order of 1 rad/sec. It dominates the angle-of-attack and pitch rate states. From a handling and control perspective, the short period dynamics have a greater influence on the quality of flight than the phugoid [25]. The aircraft model used in this analysis is a linear, two state short period approximation of longitudinal dynamics.

A short period model for the NASA X-15 hypersonic aircraft is taken from Ref. [26]. The X-15 was an experimental rocket propelled aircraft flown in the 1960s. This particular aircraft model in closed-loop with MRAC has been studied previously and analyzed for robustness. In the interest of proper comparison of results from different analyses, the same aircraft model and MRAC are used in this thesis as in past research [26]. The short period model for the X-15 is given in the standard

state-space format by the system in Eq. [2.1](#).

$$\begin{aligned}\dot{x} &= A_\lambda x + Bu \\ y &= Cx\end{aligned}\tag{2.1}$$

The states of the system in Eq. [2.1](#) are angle-of-attack α and pitch rate q , given by $x = [\alpha \text{ (deg)}, q \text{ (deg/sec)}]^T$. The input to the system is elevator deflection $u = \delta_{elev} \text{ (deg)}$. The output is the angle-of-attack $y = \alpha \text{ (deg)}$. λ denotes parametric model uncertainty. The subscript λ on the state matrix A denotes the dependence of the state matrix on this parametric uncertainty.

More specifically, the state, input, and output matrices for the X-15 short period model are defined with Eq. [2.2](#) through Eq. [2.4](#).

$$A_\lambda = \begin{bmatrix} -0.2950 & 1.0000 \\ -13.0798\lambda_\alpha & -0.2084\lambda_q \end{bmatrix}\tag{2.2}$$

$$B = \begin{bmatrix} 0 \\ -9.4725 \end{bmatrix}\tag{2.3}$$

$$C = \begin{bmatrix} 1 & 0 \end{bmatrix}\tag{2.4}$$

The aircraft model is given the symbol P_λ , indicating that it is an uncertain system. The parameter λ has the structure $\lambda = [\lambda_\alpha, \lambda_q]^T$. It models uncertainty in two aerodynamic coefficients. The uncertainty enters directly into the derivative calculation of pitch rate. Angle-of-attack is only affected through coupling in the equations. In robust control theory, this structure represents a type of parametric uncertainty [27](#). Defining an appropriate parameter space for the uncertainty is required for analysis. 100 % parametric uncertainty is considered by allowing λ to vary freely on the interval $[0 \ 2]$. It is important to note that the short period dynamics remain stable throughout the entire uncertainty envelope. However, the dynamics are marginally stable for $\lambda = 0$.

The nominal model, denoted as A_{nom} , corresponds to $\lambda_\alpha = 1$ and $\lambda_q = 1$. Eigenvalue decomposition of the nominal state matrix reveals that the short period mode has a damping ratio $\zeta = 0.07$ at a frequency of 3.63 rad/sec. Indeed, the short period dynamics are lightly damped. One of the goals of the control design is to reduce the amplification of the oscillations corresponding to this mode.

2.2 Model Reference Adaptive Control

One of the most basic and intuitive architectures for adaptive systems is direct model reference adaptive control (MRAC) [28]. The simplicity of MRAC makes it suitable for demonstrating capabilities of nonlinear analysis tools for evaluating robustness, and its intuitive structure makes its behavior predictable. Although the MRAC is simple and intuitive, its dynamics are inherently nonlinear. This renders classical tools for robustness analysis useless. For example, a control system with MRAC cannot be analyzed using gain and phase margins to determine robustness. Hence, the short period aircraft model with MRAC presents a fitting example problem for nonlinear robustness analysis.

The MRAC used in this analysis is taken directly from Ref. [26]. This is a well-researched implementation of MRAC for longitudinal aircraft dynamics. The motivation for selecting this particular controller is the ability to use past robustness results as benchmarks for evaluating the new analysis tools. With data available for comparison, it is possible to make claims about the capabilities and effectiveness of the new approach.

The MRAC has four main components: a reference model, an adaptive law, and two constant gain blocks. The resulting sub-system is nonlinear, adaptive, and produces the control signal u . The system interconnection is shown in Fig. 2.1. Note that signal ref is the α reference command, x is the aircraft state, and y is the output α .

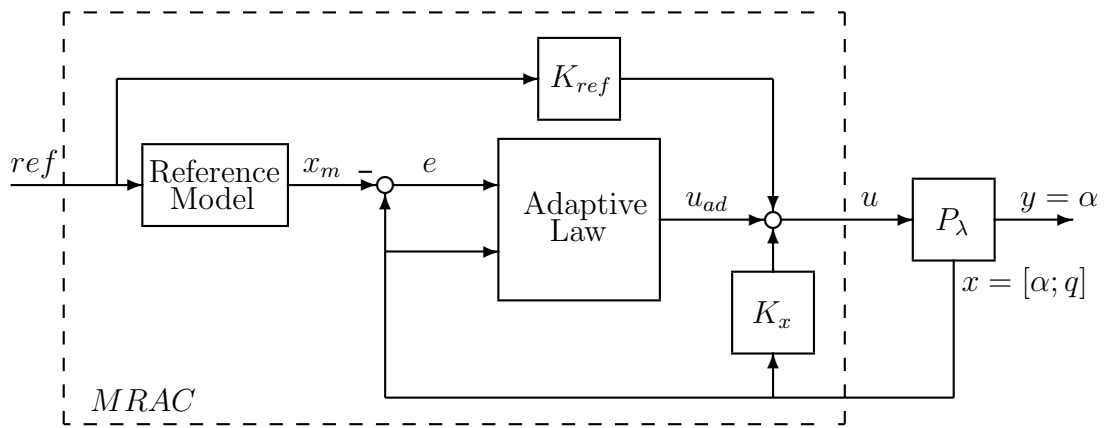


Figure 2.1: System interconnection for aircraft model with MRAC.

From the system interconnection diagram in Fig. 2.1, the control signal u is a summation of three separate components. These components originate from the state feedback block K_x , the reference feedforward block K_{ref} , and the adaptive law block. The resulting signal u is the input to the aircraft model P_λ . Accordingly, the control law is defined by Eq. 2.5.

$$u = K_x x + K_{ref} ref + u_{ad} \quad (2.5)$$

The state feedback term K_x is designed first. It is a constant gain matrix in full-state feedback with the aircraft model P_λ . It is designed as a stability augmentation system to increase damping in the short period oscillatory mode of the nominal model. The controller is designed using the LQR method, minimizing the cost function J in Eq. 2.6.

$$J = \int x(t)^T R_1 x(t) + u(t)^T R_2 u(t) dt \quad (2.6)$$

In the cost function J , the parameter weights R_1 and R_2 are selected as I_2 and 1, respectively. The resulting matrix K_x is shown in Eq. 2.7. Note that the Matlab LQR solver assumes negative state feedback. For consistency with the interconnection in Fig. 2.1, which shows to have positive feedback, a negative sign is included directly in the matrix K_x .

$$K_x = \begin{bmatrix} 0.0577 & 0.9843 \end{bmatrix} \quad (2.7)$$

The LQR result is intuitive from a qualitative standpoint. Aircraft dynamics have historically been defined with the property that a positive actuator deflection results in a negative response [25]. Due to this negative sign inherent to aircraft dynamics, positive feedback is required when implementing control. This corresponds to the positive entries in K_x and the positive feedback junction in Fig. 2.1. The resulting inner-loop system is overdamped with eigenvalues at -2.14 and -7.69. To aid in the design process, $G_{il}(s)$ is defined as the inner-loop transfer function. It is given by Eq. 2.8.

$$G_{il}(s) = C [sI_2 - (A_{nom} + BK_x)]^{-1} B \quad (2.8)$$

The feedforward gain K_{ref} is designed to ensure the closed-loop gain of the whole system is 1 at low frequency. As a result, the output angle-of-attack y tracks the angle-of-attack command input ref . To achieve this, K_{ref} must invert $G_{il}(0)$, resulting in a system DC gain of 1. To this end, K_{ref} is defined by Eq. [2.9](#).

$$K_{ref} = [-C(A_{nom} + BK_x)^{-1}B]^{-1} = -1.7354 \quad (2.9)$$

Finally, the control signal u is augmented with component u_{ad} , corresponding to the adaptive law. This is the central feature of the MRAC. The relationship is defined in Eq. [2.10](#).

$$u_{ad} = \theta^T x \quad (2.10)$$

In this relationship, θ is a vector of adaptation parameters. If the adaptation parameters were constant, this augmentation would be a time-invariant stability augmentation system like K_x . However, the adaptation parameters are states of a dynamical system. This dynamical system is called the parameter update law, and is defined in Eq. [2.11](#).

$$\dot{\theta} = -\kappa x e^T P B - \sigma \theta \quad (2.11)$$

These dynamic gains in the feedback loop give rise to a nonlinear adaptive control system. The adaptive law is a function of the aircraft state x and the error signal e . Signal e is the difference between state x and the reference model state x_m . The reference model is defined as the nominal aircraft model in feedback with K_x and with K_r as a feedforward gain. In other words, the reference model is the transfer function $K_r G_{il}(s)$. The system in Eq. [2.12](#) summarizes the structure of the reference model.

$$\begin{aligned} \dot{x}_m &= (A_{nom} + BK_x)x_m + BK_r u \\ &= A_m x_m + B_m u \\ y_m &= C x_m \end{aligned} \quad (2.12)$$

Given these definitions, signal e is a characterization of deviation from the nominal aircraft model by the true model. This error is the main driver in the adaptive law. If the aircraft model has no uncertainty, x and x_m are identically equal to each other. In

this case, the adaptive law is deactivated since the error is zero. Hence, the adaptive law is actually driven by uncertainty in the aircraft model.

There are two tuning parameters in the parameter update law given by Eq. 2.11, κ is the adaptation gain, and σ is the sigma modification gain. The adaptation gain sets how quickly the θ dynamics evolve. The sigma modification gain adds robustness to the system by ensuring boundedness of the θ parameters. In the analysis, κ and σ are varied and robustness of the closed-loop is also examined.

The symmetric matrix variable P in Eq. 2.11 is a control design parameter. It is calculated by solving the Lyapunov equation $A_m^T P + P A_m = -Q$, where $Q = 2I_2$. Details on the selection of P are provided in the next section. The value of P used in the control design is shown in Eq. 2.13.

$$P = \begin{bmatrix} 1.8136 & 0.0341 \\ 0.0341 & 0.1085 \end{bmatrix} \quad (2.13)$$

With these components, the MRAC is fully defined. It is a nonlinear system with adaptive gains. The adaptation parameters attempt to estimate uncertainty in the aircraft model, and drive the closed-loop dynamics towards the nominal condition. The next section highlights a few important points about the MRAC.

2.3 Key Properties of the Closed-Loop System

A major assumption is made about the uncertainty in the aircraft model. It is assumed that the uncertainty is matched. Matched uncertainty is defined as uncertainty belonging to the range space of the control authority. It can be completely accounted for and eliminated with a properly selected control signal. More precisely, it is assumed that for all uncertainties λ , there exists an ideal gain θ^* such that $A_\lambda + B(K_x + \theta^{*T}) = A_m$. From this relation, the ideal gain is derived in Eq. 2.14.

$$B\theta^{*T} = A_m - A_\lambda - BK_x = A_{nom} - A_\lambda \quad (2.14)$$

The value of θ^* depends on λ , meaning that the optimal gain depends on the particular value of the uncertainty. The $B\theta^{*T}$ term is a direct measure of deviation from the nominal state matrix by the uncertain state matrix. For the nominal case, where $A_\lambda = A_{nom}$, it is clear that θ^* is zero. Hence, adaptation is not required.

For convenience, define the parameter error as $\tilde{\theta} = \theta - \theta^*$. This represents the difference between actual adaptive gain and ideal gain for any particular uncertainty value. Given the definition of error signal $e = x - x_m$, the error dynamics for the full MRAC system in closed-loop are derived. These error dynamics are summarized in Eq. [2.15](#).

$$\begin{aligned}
\dot{e} &= \dot{x} - \dot{x}_m \\
&= (A_\lambda + BK_x + B\theta^T)x + BK_{ref}ref - (A_mx_m + B_mref) \\
&= (A_\lambda + BK_x + B\theta^T)x + BK_{ref}ref - A_mx_m - BK_{ref}ref \\
&= (A_\lambda + BK_x + B\theta^T)x - A_mx_m \\
&= (A_\lambda + BK_x + B\theta^{*T})x - A_mx_m + B\theta^T x - B\theta^{*T}x \\
&= A_mx - A_mx_m + B\theta^T x - B\theta^{*T}x \\
&= A_me + B\tilde{\theta}^T x
\end{aligned} \tag{2.15}$$

Letting $P = P^T > 0$, and solving the Lyapunov equation $A_m^T P + PA_m = -Q$ for any $Q > 0$ yields a meaningful stability result. Consider the Lyapunov function candidate in Eq. [2.16](#) where $\kappa > 0$ is a scalar constant.

$$V = e^T P e + \frac{1}{\kappa} \tilde{\theta}^T \tilde{\theta} \tag{2.16}$$

The time derivative function \dot{V} is calculated in Eq. [2.17](#) using the error dynamics from Eq. [2.15](#) and the parameter update law in Eq. [2.11](#). To first show a notable result for purely adaptive systems without sigma modification, the sigma modification term in the parameter update law is neglected.

$$\begin{aligned}
\dot{V} &= \dot{e}^T P e + e^T P \dot{e} + \frac{1}{\kappa} \dot{\tilde{\theta}}^T \tilde{\theta} + \frac{1}{\kappa} \tilde{\theta}^T \dot{\tilde{\theta}} \\
&= [A_me + B\tilde{\theta}^T x]^T P e + e^T P [A_me + B\tilde{\theta}x] - B^T P e x^T \tilde{\theta} - \tilde{\theta}^T x e^T P B \\
&= e^T [A_m^T P + PA_m] e + x^T \tilde{\theta} B^T P e + e^T P B \tilde{\theta}^T x - B^T P e x^T \tilde{\theta} - \tilde{\theta}^T x e^T P B \\
&= -e^T Q e
\end{aligned} \tag{2.17}$$

Note that the terms $x^T \tilde{\theta}$ and $\tilde{\theta}^T x$ in the derivation are scalar. Hence, they commute within their respective terms. Using this property, the cross terms in the derivation cancel, leading to the result in Eq. [2.17](#).

The structure of Eq. [2.17](#) is a standard adaptive control stability result [\[28\]](#). The function \dot{V} is only negative semidefinite, since the adaptation parameters do not appear explicitly in the final result. Convergence of e to the origin follows from Lyapunov theory and Barbalat's Lemma. However, no conclusion is drawn about the convergence of the adaptation parameters [\[29\]](#).

The sigma modification term in Eq. [2.11](#) is used in the parameter update law to ensure boundedness of the adaptation parameters [\[28\]](#). The time derivative function \dot{V} is recomputed using the sigma modified adaptive law, and shown in Eq. [2.18](#)

$$\dot{V} = -e^T Q e - \frac{2\sigma}{\kappa} \tilde{\theta}^T \theta \quad (2.18)$$

Eq. [2.18](#) is not negative semidefinite for small values of e , since the second term is not sign definite. Hence, the inclusion of sigma modification in the dynamics renders the original Lyapunov function candidate useless in proving stability. It is a known result that sigma modification increases robustness at the expense of the precise convergence of e to the origin. However, all signals remain bounded, and e converges to a small closed region near the origin [\[28\]](#).

The nonlinear analysis approach used in the forthcoming sections can only be applied to systems governed by polynomial dynamics. The short period MRAC closed-loop is a polynomial model. There are two polynomial sub-systems in the MRAC. The MRAC's parameter update law in Eq. [2.11](#) includes a product of x and e . Expanding e , the parameter update law has two nonlinear terms. The first is governed by xx^T , and the second by xx_m^T . Note that these nonlinear terms are polynomial. The MRAC control signal's adaptive component u_{ad} defined in Eq. [2.10](#) is also nonlinear and polynomially governed by the product of $\theta^T x$. The remaining components in the closed-loop system are linear. The aircraft model is linear, as are the constant gains and the reference model. A key observation is that the MRAC closed-loop system is a polynomial system. It can be written in the form shown by the system in Eq. [2.19](#).

$$\begin{aligned} \dot{z} &= f(z, ref) \\ y &= h(z, ref) \end{aligned} \quad (2.19)$$

In Eq. [2.19](#), $z = [\theta, x_m, x]^T$ is the MRAC state augmented with the aircraft state, and ref is the input. The output y is still the angle-of-attack. Given the system

dynamics, f and h are polynomial functions.

Chapter 3

Sum-of-Squares Optimization

The underlying mathematical theory behind the analysis approach in this thesis is related to the properties of sum-of-squares (SOS) polynomials. This section provides a brief review of SOS polynomials and the optimizations that exploit their properties. Background and more detailed information can be found in Refs. [1–3].

A polynomial p is said to be SOS if there exist polynomials $\{f_i\}_{i=1}^m$ such that $p = \sum_{i=1}^m f_i^2$. For example, $p = x^2 - 4xy + 7y^2$ is SOS because $p = f_1^2 + f_2^2$, where $f_1 = (x - 2y)^2$ and $f_2 = 3y^2$. Note that any SOS polynomial is a globally positive semidefinite function. The sign definite property of these polynomials will be used in a particular way to construct Lyapunov functions and make arguments about the stability of a system.

Quadratic form polynomials can be always be expressed in the form $p(x) = x^T Q x$, where Q is a symmetric matrix. Similarly, polynomials of degree $\leq 2d$ can be expressed as $p(x) = z(x)^T Q z(x)$, where the vector z contains all monomials of degree $\leq d$. This is commonly known as the Gram matrix form. In general, the Gram matrix Q is not unique. For a given polynomial p , there may exist many Q which satisfy the equality. A key and very useful property is that $p(x)$ is an SOS polynomial if and only if there exists a symmetric positive semidefinite matrix Q such that $p(x) = z(x)^T Q z(x)$. This property is a vital connection between SOS polynomials and positive semidefinite matrices.

An SOS program is an optimization problem with a linear cost and SOS constraints on the decision variables [21]. The optimization problem is summarized by the statement

in Eq. [3.1](#).

$$\begin{aligned} \min_{u \in \mathbb{R}^n} c^T u & \tag{3.1} \\ a_{k,0}(x) + a_{k,1}(x)u_1 + \dots + a_{k,n}(x)u_n \in \text{SOS} & \quad (k = 1, \dots, N_s) \end{aligned}$$

The vector $c \in \mathbb{R}^n$ and polynomials $a_{k,j}$ are specified as part of the optimization setup. $u \in \mathbb{R}^n$ is the vector of decision variables found by the optimization. SOS programs can be converted to semidefinite programs (SDP) using the connection between SOS polynomials and positive semidefinite matrices. SOSTOOLS [\[21\]](#), Yalmip [\[22\]](#), and SOSOPT [\[23\]](#) are freely available MATLAB toolboxes for solving SOS optimizations. In particular, SOSOPT is used in this analysis. These packages allow the user to specify the polynomial constraints using a symbolic toolbox. They convert the SOS optimization into an SDP, which is solved with SeDuMi [\[30,31\]](#) or another SDP solver. Finally, the solution of the SDP is converted back to a polynomial solution.

A major drawback of this approach is the rapid increase in size of the resulting SDP as a function of the number of variables and the polynomial degree. For a generic degree $2d$ polynomial with n variables, the Gram matrix representation involves $l_z = \binom{n+d}{d}$ monomials. An SOS constraint is enforced via the positive semidefinite constraint on Q , which is an $l_z \times l_z$ Gram matrix. For example, Q has dimension $l_z = 495$ for a generic degree 8 polynomial in 8 variables. The size of this matrix constraint is near the limits of current SDP solvers. The problem structure can be exploited [\[32\]](#), but this computational growth is a generic trend in SOS optimizations. For analysis of polynomial systems, this roughly limits the approach to systems with fewer than 8-10, states and cubic degree models. Polynomial models of higher degree can be handled if there are fewer states.

As mentioned previously, SOS polynomials are globally positive semidefinite. Lyapunov based analysis is generally centered around satisfying non-negativity conditions on functions and their time derivatives, which involve the governing system dynamics. If the Lyapunov function candidate is polynomial, stability certificates can be obtained using SOS optimization. This SOS approach is ideally suited for control systems governed by polynomial dynamics. For problems involving non-polynomial dynamics, they must be approximated as such.

Many types of nonlinear analysis problems can be formulated as polynomial opti-

mization problems with SOS constraints. Some of these include estimating regions of attraction, reachability sets, local input-output gains, input-output gains with other signal norms, robustness with respect to parametric uncertainty, and time delay margin [4-20]. The analysis in this thesis focuses on estimating time delay margin for the MRAC system. This SOS optimization is applicable because the MRAC closed-loop system is governed by polynomial dynamics.

Chapter 4

Stability Analysis

The notion of linear robustness metrics, such as gain and phase margin, do not extend to nonlinear systems. Even for the case of polynomial dynamics, more advanced approaches for evaluating robustness to uncertainty are required. A logical extension of the phase margin for nonlinear systems is the time delay margin. In real systems, where transport or telemetry delay are often quantifiable measures, knowledge of the time delay margin is crucial to making claims about stability and robustness. An approach to estimating the time delay margin for polynomial systems using SOS optimization was proposed in Ref. [19] and refined in Ref. [20]. In this chapter, the approach in Ref. [19] is derived in detail towards the analysis of the MRAC aircraft system.

4.1 Global Stability Conditions

Common practices towards estimating the time delay margin for nonlinear systems rely on exhaustive Monte Carlo simulations. Such approaches lack the rigor and strength of robustness analysis tools available for linear systems. An analytical and more rigorous approach is desired for nonlinear systems. To develop this approach, it is first assumed that the system dynamics can be reduced to a model of the form in Eq. [4.1].

$$\dot{x}(t) = f(x(t), x(t-r)) \tag{4.1}$$

In this model, $x(t)$ is the current state vector, and $x(t-r)$ is the delayed state vector. The function f is an $n_x \times 1$ vector-valued polynomial function of $x(t)$ and $x(t-r)$ such that $f(0,0) = 0$. Implicitly, this system is infinite dimensional. The current derivative depends explicitly on the current state and the delayed state. However, knowledge of the entire state vector time history on the time delay interval is required for predicting future states. This infinite dimensional time history is denoted $x(m)$, where $m \in [t-r, t]$. Although restricting the model to this structure appears limiting, many real systems can be modeled in this way. Controller computation, communication, and transport delay are examples of delays in systems representable by Eq. [4.1](#)

Time delay systems with finite time delay margins are said to be delay-dependent stable. In such systems, there exists a time delay r large enough to cause instability. This is analogous to a finite phase margin in linear systems. The largest r for which the system is stable is defined as the time delay margin. The largest r for which stability can be numerically certified is a lower bound of that margin.

A set of Lyapunov conditions is formulated for analyzing the stability of polynomial systems with time delay. This set of conditions is used to calculate a lower bound on the time delay margin. The conditions are satisfied by numerically certifying their global non-negativity for time delays up to size r . If satisfied, the system is guaranteed to be stable for time delays up to size r . The lower bound of the time delay margin is calculated by attempting to certify the conditions through a bisection algorithm on r .

The dynamics in Eq. [4.1](#) are assumed to be nonlinear and polynomial. Therefore, the quadratic form Lyapunov functions used in linear analysis are not sufficient to guarantee stability. A more complex Lyapunov function candidate is proposed in Eq. [4.2](#). Specifically, it is a functional because its argument is $x(m)$. Eq. [4.2](#) maps a vector space $x(m)$ into real numbers.

$$V(x(m)) = V_0(x(t)) + \int_{-r}^0 V_1(\tau, x(t), x(t+\tau)) d\tau + \int_{-r}^0 \int_{t+\tau}^t V_2(x(\xi)) d\xi, d\tau \quad (4.2)$$

In Eq. [4.2](#), the functions V_0 , V_1 , and V_2 are polynomials. The polynomial functional $V(x(m))$ depends on the current state and the entire interval of the state trajectory inside the window of the time delay. For systems without time delay, V_0 alone would be a logical choice of Lyapunov function candidate. The integral terms are included

to account for the time delay. Note that the integration bounds correspond to the time delay interval.

The function V must be positive definite to show stability with Lyapunov theory. Positive definiteness of each term is sufficient but not necessary. Given at least one positive definite term, the others can be positive semidefinite. V_0 is constrained to be positive definite, allowing slack in the remaining terms. The kernels of the integral terms are constrained to be positive semidefinite. Indeed, the integral of a positive semidefinite function is positive semidefinite itself.

The time derivative \dot{V} must also be negative semidefinite to ensure stability with Lyapunov theory. Arriving at an elegant form of this derivative from V is not straightforward. In particular, the derivative of the second term V_1 requires algebraic manipulation, shown in the derivation arriving at Eq. [4.3](#).

$$\begin{aligned}
\frac{d}{dt} \int_{-r}^0 V_1 d\tau &= \int_{-r}^0 \frac{\partial V_1}{\partial \tau} \frac{d\tau}{dt} + \frac{\partial V_1}{\partial x(t)} \frac{dx(t)}{dt} + \frac{\partial V_1}{\partial x(t+\tau)} \frac{dx(t+\tau)}{dt} d\tau \\
&= \int_{-r}^0 \frac{\partial V_1}{\partial x(t)} f + \frac{\partial V_1}{\partial x(t+\tau)} \frac{dx(t+\tau)}{d\tau} d\tau \\
&= \int_{-r}^0 \frac{\partial V_1}{\partial x(t)} f + \frac{\partial V_1}{\partial x(t+\tau)} \frac{dx(t+\tau)}{d\tau} + \frac{\partial V_1}{\partial \tau} - \frac{\partial V_1}{\partial \tau} d\tau \\
&= \int_{-r}^0 \frac{\partial V_1}{\partial x(t)} f - \frac{\partial V_1}{\partial \tau} d\tau + \int_{-r}^0 \frac{\partial V_1}{\partial x(t+\tau)} \frac{dx(t+\tau)}{d\tau} + \frac{\partial V_1}{\partial \tau} d\tau \\
&= \int_{-r}^0 \frac{\partial V_1}{\partial x(t)} f - \frac{\partial V_1}{\partial \tau} d\tau + \int_{-r}^0 \frac{dV_1}{d\tau} d\tau \\
&= \int_{-r}^0 \frac{\partial V_1}{\partial x(t)} f - \frac{\partial V_1}{\partial \tau} d\tau + V_1(0, x(t), x(t)) - V_1(-r, x(t), x(t-r)) \quad (4.3)
\end{aligned}$$

Taking the derivative of the first and third terms in V is straightforward. With the result in Eq. [4.3](#), the full time derivative of V is composed and shown in Eq. [4.4](#).

$$\begin{aligned}
\frac{d}{dt} V &= \frac{dV_0}{dx(t)} f + V_1(0, x(t), x(t)) - V_1(-r, x(t), x(t-r)) \\
&\quad + \int_{-r}^0 \frac{\partial V_1}{\partial x(t)} f - \frac{\partial V_1}{\partial \tau} + V_2(x(t)) - V_2(x(t+\tau)) d\tau \quad (4.4)
\end{aligned}$$

Note that the terms outside the integral in Eq. [4.4](#) have no dependence on the variable of integration. For simplicity, they can be included in the integral term with a scaling

factor $\frac{1}{r}$. Hence, the derivative of V can be expressed as a single integral. This is desirable because its kernel can easily be constrained to be negative semidefinite by the same logic that constrained the kernels of the integral terms in V .

A set of sufficient conditions for global stability of the polynomial time delay system in Eq. [4.1](#) is formulated in Lemma [1](#). The structure of V defined in Eq. [4.2](#) is the foundation of this lemma.

Lemma 1 *Assume the origin is an equilibrium point for the system in Eq. [4.1](#), polynomials V_0 , V_1 , and V_2 exist, and that $\psi(x(t))$ is a positive definite polynomial function such that:*

- 1) $V_0(x(t)) - \psi(x(t)) \geq 0$
- 2) $V_1(\tau, x(t), x(t + \tau)) \geq 0 \quad \forall \tau \in [-r, 0]$
- 3) $V_2(x(\xi)) \geq 0$
- 4) $\frac{1}{r} \frac{dV_0}{dx(t)} f + \frac{1}{r} V_1(0, x(t), x(t)) - \frac{1}{r} V_1(-r, x(t), x(t - r)) + \frac{\partial V_1}{\partial x(t)} f - \frac{\partial V_1}{\partial \tau} + V_2(x(t)) - V_2(x(t + \tau)) \leq 0 \quad \forall \tau \in [-r, 0]$

then the origin is a globally stable equilibrium for time delays up to size r .

The first condition in Lemma [1](#) is equivalent to ensuring that $V_0(x(t)) \geq \psi(x(t))$. Since $\psi(x(t))$ is positive definite by definition, the inequality guarantees that V_0 is also positive definite, which is a requirement for Lyapunov stability. Rather than constraining V_0 to be positive definite directly, condition 1 is used because SOS optimization is limited to semidefinite constraints. The second and third conditions in Lemma [1](#) ensure that the kernels of the integral terms in V are positive semidefinite. Since V_0 is already positive definite, the conditions on the remaining terms can be relaxed to positive semidefinite directly. Hence, the overall positive definiteness of V is ensured. The fourth condition constrains the derivative \dot{V} to be negative semidefinite.

The next section is dedicated to transforming the inequality stability conditions in Lemma [1](#) to SOS stability conditions. As such, the stability conditions can be certified using optimization methods. The SOS conditions are then relaxed from global to local conditions. Certifying global stability is conservative for nonlinear systems,

where stability around an equilibrium point is typically a sufficient result. Global stability can even perhaps be infeasible, since multiple equilibria may exist. Guaranteed local stability inside a specified box in the system state space is often sufficient for engineering applications.

4.2 Local Sum-of-Squares Stability Conditions

Each term in the conditions of Lemma 1 is a polynomial function. However, the time delay interval restriction $\tau \in [-r, 0]$ in conditions 2 and 4 is not a polynomial object. To certify stability by SOS optimization, conditions 2 and 4 must be converted to purely polynomial constraints. Neglecting the interval restriction completely, the conditions would become valid SOS constraints. However, SOS optimization would then seek to satisfy the constraints for all values of τ . This certificate would imply stability for all time delays, which is conservative since a finite margin is expected. Instead, a variant of the S-procedure is used for constraint relaxation to create SOS conditions.

The term V_1 in condition 2 is required be positive semidefinite on the interval $\tau \in [-r, 0]$. A special polynomial function $h(\tau) = \tau(\tau + r) = \tau^2 + \tau r$ is defined. This function is negative semidefinite on the interval $\tau \in [-r, 0]$, and positive definite elsewhere. Augmenting $h(\tau)$ to condition 2, and using an SOS multiplier p_1 , the relaxed SOS constraint in Eq. 4.5 is composed.

$$V_1(\tau, x(t), x(t + \tau)) + p_1(\tau, x(t), x(t + \tau)) h(\tau) \in SOS \quad (4.5)$$

Certifying that Eq. 4.5 is SOS implies that V_1 is positive semidefinite for all $\tau \in [-r, 0]$. Since the total constraint is SOS, and $h(\tau)$ is negative semidefinite on the interval, V_1 must be positive semidefinite on the interval. Outside this interval, where the system may actually be unstable, V_1 is allowed to be negative. But outside the interval, $h(\tau)$ is positive and able to cancel out the potentially negative V_1 . The key point is that the total constraint can still be SOS without requiring that V_1 be positive definite for all values of time delay. An illustrative example of S-procedure constraint relaxation is shown in Fig. 4.1.

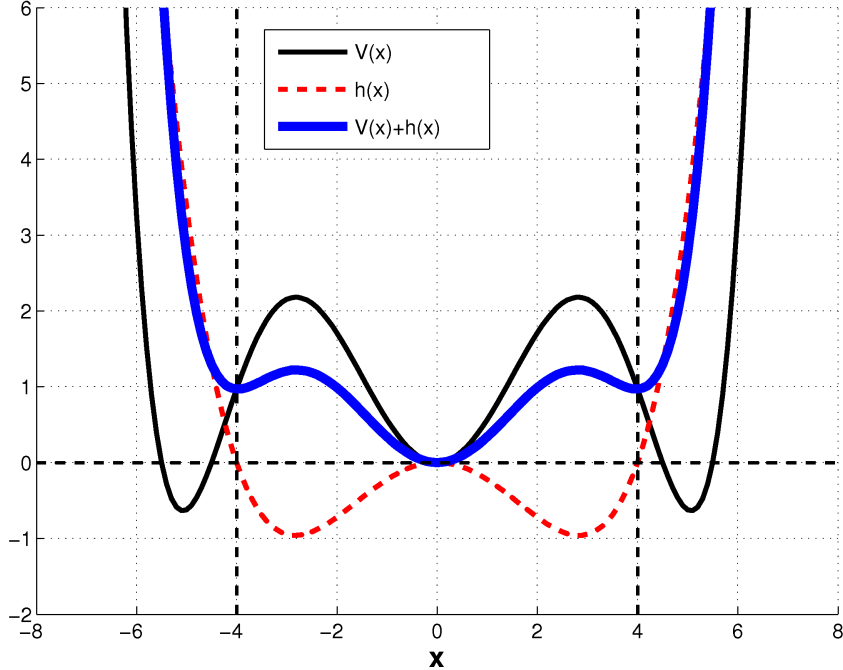


Figure 4.1: Graphical interpretation of S-procedure constraint relaxation.

For the example in Fig. 4.1, stability must be certified for $|x| \leq 4$. A Lyapunov function that is positive definite in this region must be found. The function $V(x)$ in Fig. 4.1 is positive definite in the required region and would be sufficient to prove stability. However, it would not be considered by the SOS optimization because it is not globally positive semidefinite or SOS. The function $h(x)$ is negative semidefinite for $|x| \leq 4$ and positive definite otherwise. Augmenting $V(x)$ with $h(x)$ results in a globally positive definite function. This function can therefore be constructed with SOS optimization. The existence of this constructed SOS function together with the sign conditions on $h(x)$ guarantee that $V(x)$ is positive definite in the region of interest. Hence, stability is certified for all values of $|x| \leq 4$. This type of constraint relaxation is referred to as the S-procedure.

Applying the S-procedure, the fourth condition in Lemma 1 is augmented and converted into an SOS constraint using multiplier p_2 . Since the interval restriction on τ is the same as in condition 2, the same function $h(\tau)$ is used. Conditions 2 and 4 are thus valid SOS constraints that can be certified using SOS optimization. However, these conditions still certify global stability in terms of the system state space. This is conservative, and further constraint relaxation from global to local stability is necessary.

Limiting the certification of the SOS constraints to a box in state space around the origin implies that there exists a local stability region in this box. In particular, the largest level set of the Lyapunov function fully contained in the box is an invariant set. Hence, every trajectory originating from that level set is stable. The magnitude of the box is defined by $|x_i| \leq \zeta_i$. Each x_i represents an individual state, and to allow flexibility, each direction is constrained independently in terms of ζ_i . The S-procedure is utilized again to relax the global SOS conditions into local SOS conditions.

The S-procedure augments the global conditions with a set of specially defined polynomial functions to create local conditions. These functions are similar in structure to the $h(\tau)$ function used previously. They are negative semidefinite in the local region defined by the box in state space, and positive definite elsewhere. Since $x(t)$, $x(t + \tau)$, and $x(t - r)$ are treated as separate sets of state variables in the optimization, three sets of h_{ji} functions are defined. Each state variable set is denoted with the j index. The i index is reserved for the individual state in a particular variable set. Consider the structure of h_{ji} functions shown in Eq. [4.6](#) through Eq. [4.8](#).

$$h_{1i} = (x_i(t) - \zeta_i) (x_i(t) + \zeta_i) \tag{4.6}$$

$$h_{2i} = (x_i(t + \tau) - \zeta_i) (x_i(t + \tau) + \zeta_i) \tag{4.7}$$

$$h_{3i} = (x_i(t - r) - \zeta_i) (x_i(t - r) + \zeta_i) \tag{4.8}$$

These h_{ji} polynomial functions are defined to augment V and \dot{V} , generating local constraints. Including h_{ji} functions in conditions 1 and 4 is sufficient for the augmenting terms to appear once in V and \dot{V} , respectively. Hence, the global constraints are relaxed into local constraints. The h_{ji} polynomials enter the conditions with respective SOS multiplier functions q_{ji} . The resulting local SOS conditions are sufficient to prove local stability for time delays up to a size r . The final SOS conditions are summarized with the Lemma [2](#).

Lemma 2 Assume that the origin is an equilibrium point for the system in [4.1](#), that polynomials V_0 , V_1 , and V_2 exist. Further, assume that $\psi(x(t))$ is a positive definite SOS polynomial and that p_1 , p_2 , and q_{ji} are SOS polynomials such that:

- 1) $V_0(x(t)) - \psi(x(t)) + \sum_{i=1}^n q_{1i}h_{1i}$ is SOS
- 2) $V_1(\tau, x(t), x(t + \tau)) + p_1h(\tau)$ is SOS
- 3) $V_2(x(\xi))$ is SOS
- 4) $-r \frac{\partial V_1}{\partial x(t)} f - \frac{dV_0}{dx(t)} f + r \frac{\partial V_1}{\partial \tau} - rV_2(x(t)) + rV_2(x(t + \tau)) - V_1(0, x(t), x(t)) + V_1(-r, x(t), x(t - r)) + p_2h(\tau) + \sum_{i=1}^n (q_{1i}h_{1i} + q_{2i}h_{2i} + q_{3i}h_{3i})$ is SOS

then the origin is a locally stable equilibrium for time delays up to size r .

The conditions in Lemma [2](#) are local SOS constraints that can be checked with SOS optimization. A bisection algorithm on values of r calculates a lower bound on the time delay margin for the system. The bisection is necessary because the fourth constraint is bilinear in the decision variables. The unknown r and the coefficients of V_1 and V_2 enter the fourth condition bilinearly.

Chapter 5

Problem Formulation

Up to this point in the thesis, two distinct topics have been explored. First, an aircraft model implementing a simple MRAC was defined. This model is a nonlinear adaptive control system governed by polynomial dynamics. Then, a theoretical approach to nonlinear robustness analysis was outlined. This approach relies on SOS optimization to calculate a lower bound on time delay margin for polynomial systems. What remains is the unification of these two related, yet still disjoint, topics. This chapter focuses on casting MRAC robustness analysis as a properly formulated SOS optimization problem.

Time delay margin is a crucial robustness metric for the closed-loop MRAC system. A guaranteed lower bound for this stability margin is required before the architecture can be implemented safely. The goal of this analysis is to use SOS optimization to satisfy the conditions in Lemma 2 for the MRAC system. This would guarantee the stability of the system in the presence of a particular time delay.

A pure time delay of magnitude τ seconds is introduced in the system dynamics between the controller and the aircraft model. This time delay can be interpreted physically as a computation, sampling, or network delay. A single time delay is considered in the dynamics for simplicity. Fig. 5.1 shows the time delayed MRAC closed-loop system architecture. The only update to this diagram is that the control signal u is delayed by τ seconds before reaching the aircraft model.

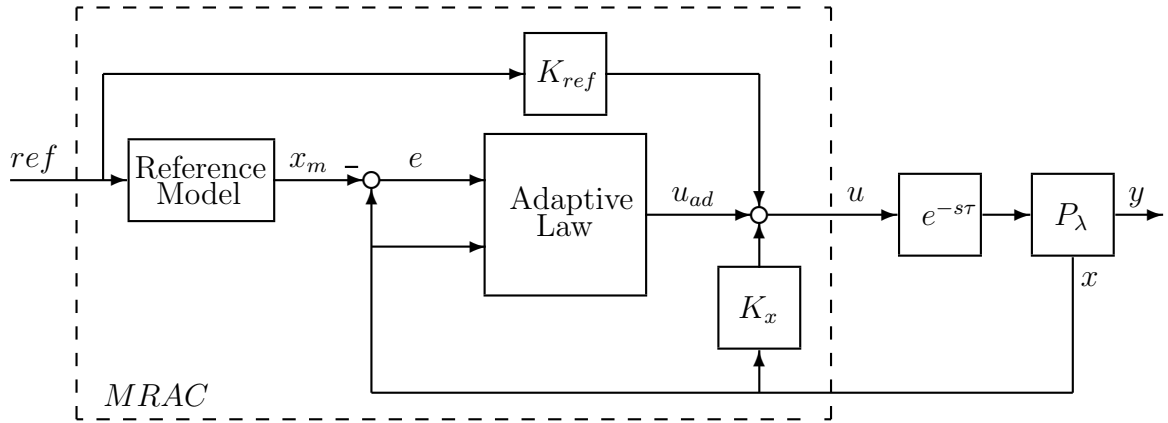


Figure 5.1: System interconnection for time delayed aircraft model with MRAC.

The diagram in Fig. 5.1 indicates the location of the time delay in the MRAC closed-loop system interconnection. The control signal is delayed by τ seconds before reaching the aircraft model.

A final point must be addressed before SOS optimization can be applied to this system. Recall from the derivation of the stability analysis that the model is assumed to take the form of Eq. 4.1. Thus, it is required that that model is an autonomous system. The input signal ref must be neglected in the dynamics to satisfy this condition. What remains is an autonomous polynomial system modeled by Eq. 4.1. Hence, the SOS optimization aims to certify the stability of a local set of initial conditions in the presence of time delay for the MRAC system.

Neglecting the input signal ref may appear limiting for a nonlinear system. The choice of input and its size can generally lead to degradation of stability margins in nonlinear systems. In the case of the MRAC system, however, analysis with the particular input choice $ref = 0$ still leads to insightful results. The input $ref = 0$ is just one selection from the set of all possible inputs. Analysis resulting from this particular input choice serves as a best-case scenario for robustness margins. It is not possible to increase the set of valid inputs and gain improvement in margins. Considering non-zero input signals can only degrade the time delay margin found for $ref = 0$.

The absence of the input signal ref alters the MRAC system dynamics. The effect of the feedforward gain K_{ref} is completely eliminated. The reference model state x_m is

also zero for all time. This change implies that the error signal e is always equivalent to the true aircraft state x , altering the parameter update law. The parameter update law in the absence of the reference signal is shown in Eq. 5.1. Note that the adaptive term is governed by the quadratic term xx^T , instead of xe^T .

$$\dot{\theta} = -\kappa xx^T P B - \sigma \theta \quad (5.1)$$

The simplified system dynamics are represented by an updated interconnection, shown in Fig. 5.2. Although the system dynamics are different from the original MRAC, a key point is that the new dynamics remain polynomial. Hence, their robustness properties can be analyzed with the proposed SOS optimization.

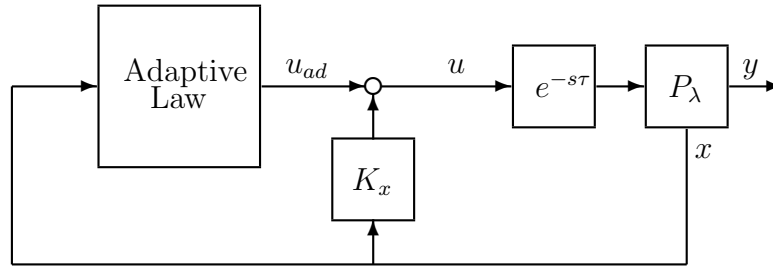


Figure 5.2: Simplified system interconnection neglecting input reference signal.

SOS optimization attempts to construct a Lyapunov function sufficient to prove local stability in the presence of time delay. This optimization is performed on the MRAC system dynamics where the input reference signal ref is neglected. The construction of such Lyapunov functions is not at odds with known results about MRAC systems with sigma modification. Recall that the simple Lyapunov function V in Eq. 2.16 could not prove stability even in the absence of time delay due to the effects of sigma modification. Proving stability for the system without delay was not possible. Thus, attempting to prove stability with delay in the system does not follow. However, the inability to prove stability occurred under the assumption that a reference signal existed. Omitting the reference signal, the dynamics change. It then becomes trivial to construct quadratic Lyapunov functions that show convergence of both e and θ to the origin in the absence of time delay. The key point is that constructing simple Lyapunov functions for asymptotic convergence in the absence of time delay is possible when the reference signal is omitted. Similarly, SOS optimization extends this by constructing Lyapunov functions for asymptotic convergence in the presence

of time delay.

For the SOS optimization, a box in the MRAC closed-loop system's state space must be defined for which the stability conditions in Lemma 2 are satisfied. Ideally, this box should be as big as possible yet remain fully contained in the nonlinear system's stable region around the origin. If not entirely contained, it is not feasible to construct Lyapunov functions proving local stability. However, the size of this stable region is unknown for the MRAC system. Monte Carlo simulations of the nominal, undelayed closed-loop system provide insight into the size of the region. Initial conditions in the aircraft state are randomly selected, while the adaptation parameters are initialized at zero. For the MRAC design, the value 1 is selected for the adaptation gain and sigma modification. Fig. 5.3 suggests that trajectories originating from randomly sampled initial conditions inside a particular box of the aircraft state space are stable.

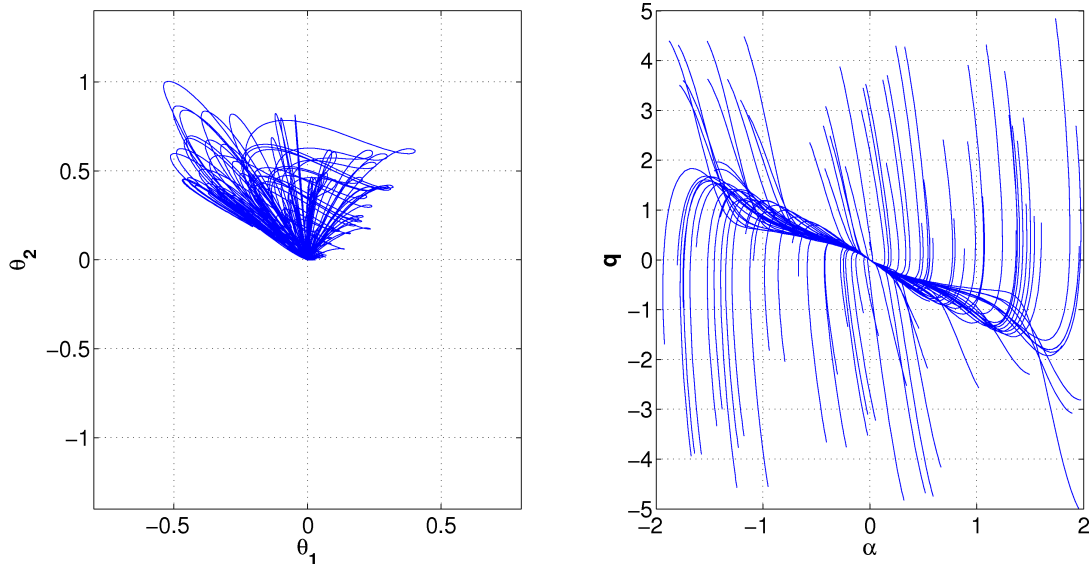


Figure 5.3: Randomly selected initial condition trajectories.

In Fig. 5.3, trajectories of the adaptation parameters are shown on the left, and trajectories of the aircraft state are shown on the right. The results indicate that the locally stable region is at least ± 2 deg on α and ± 5 deg/sec on q . These dimensions are used to define the corresponding box in the aircraft state space. The definition of a box in the adaptation parameter θ space is also required. Based on the results in Fig. 5.3, trajectories of the two states in the parameter update law satisfy a box constrained by ± 0.8 and ± 1.4 in each direction, respectively. Together, the four



state space constraints form a four dimensional box that contains all admissible initial conditions and their trajectories.

The SOS optimization constructs a Lyapunov function valid inside the defined box in the closed-loop state space by satisfying the conditions in Lemma 2. However, this result does not prove that the entire box is a locally stable region. Lemma 2 only guarantees that V is positive definite, and that \dot{V} is negative semidefinite in the box. To find the guaranteed locally stable region, the Lyapunov function must be characterized by its level sets. Consider Fig. 5.4 as an illustrative example. For this example, a two dimensional slice of the four dimensional state space is shown.

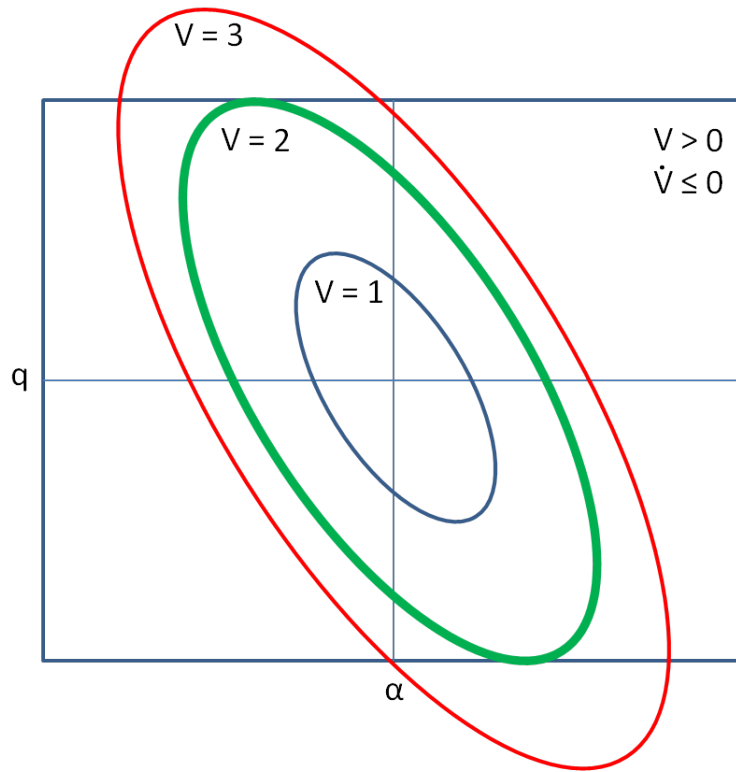


Figure 5.4: Level sets of Lyapunov function and box in state space.

Fig. 5.4 illustrates the box defined in α and q state space. Note that V is positive definite and that \dot{V} is negative semidefinite in the box. The largest level set of the Lyapunov function fully contained in the box is the guaranteed locally stable region. That level set is labeled $V = 2$ in Fig. 5.4. Trajectories originating from this region are stable, and the region comprises an invariant set for the closed-loop system. The illustrative example in Fig. 5.4 displays the largest level set of the Lyapunov function

in two dimensional space. The actual Lyapunov function for the MRAC system has four dimensions.

Chapter 6

Results

Time delay margin analysis is useful for the verification of robustness requirements in nonlinear systems. The MRAC closed-loop aircraft system is nonlinear, hence a direct method for calculating the time delay margin exactly does not exist. The SOS optimization approach is used to find a lower bound on the margin. Monte Carlo simulations provide an upper bound. Since the exact margin is unknown, both the upper and lower bounds are needed for analysis. The lower bound is meaningful if falls above the minimum required value of time delay margin, certifying the robustness requirement. Conversely, the upper bound is meaningful if falls below the requirement. It cannot be determined if the requirement has been met if the bounds straddle the requirement. In this case, however, the bounds can provide qualitative insight into trends in the time delay margin evaluated over a certain parameter space.

A reasonable minimum time delay margin requirement for the MRAC closed-loop system is inferred from the open-loop aircraft model. This requirement scales with the bandwidth of the closed-loop system. However, since the controller does not aim to alter the bandwidth, the requirement can be approximated directly from the open-loop aircraft model. The frequency response of the open-loop aircraft transfer function from elevator input δ_{elev} to angle-of-attack output α is shown in Fig. 6.1. The frequency response of the inner-loop transfer function $G_{il}(s)$ for the same input-output pair is also shown. Recall that the inner-loop is designed with full state feedback to increase damping.

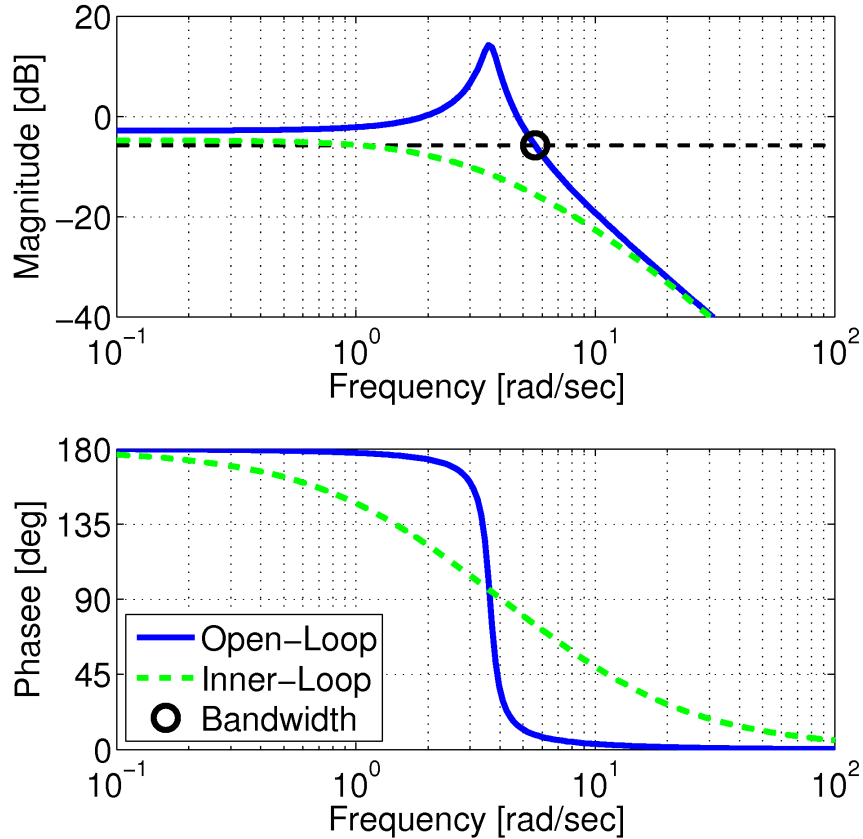


Figure 6.1: Bode plot of open-loop aircraft model and inner-loop.

The results in Fig 6.1 confirm that the inner-loop controller increases damping in the closed-loop system. The inner-loop has slightly lower bandwidth than the open-loop, but generally the same low and high frequency characteristics. Bandwidth is roughly estimated by the frequency at which the magnitude of a transfer function drops under 3 dB below DC gain [33]. This frequency is indicated for the open-loop aircraft by the highlighted point at 5.6 rad/sec in Fig 6.1. A typical performance and robustness phase margin requirement at the system bandwidth is 45 deg [33]. At 5.6 rad/sec, this requirement translates to a time delay margin of about 140 msec. Thus, a reasonable minimum time delay margin requirement for the MRAC closed-loop system is also 140 msec.

The parameter update law in the MRAC is tuned by adjusting the adaptation gain and sigma modification. Tuning the parameter update law determines the adaptive contribution to the MRAC control signal. If the adaptive component is turned off, the MRAC becomes a linear system. Hence, the full closed-loop system is linear, and a

precise time delay margin can be calculated. This time delay margin is calculated using the loop transfer function $L(s) = K_x P(s)$, in which the aircraft model is assumed to be nominal. With adaptation turned off, the time delay margin for the system is around 151 msec. This calculated margin exceeds the minimum requirement of 140 msec.

The calculation of time delay margin is desired for the MRAC closed-loop system with active adaptation. The following sections explore the effects on time delay margin by tuning the parameter update law. Specifically, the effects due to variation in the adaptation rate and sigma modification are examined. The effects due to uncertainty in the aircraft model are also analyzed. The results are interpreted in terms of trends in the upper and lower bounds and the satisfaction of the minimum time delay margin requirement.

6.1 Adaptation Rate

The central feature of the MRAC architecture is the adaptive term in the parameter update law. The adaptive term is tuned by adjusting the adaptation rate κ . This determines the rate of adaptation in the parameter dynamics. However, selecting an appropriate adaptation rate is not intuitive because the adaptive term is nonlinear.

Simulations are used to gain intuition of the effects of varying the adaptation rate on the closed-loop response of the aircraft. Initial conditions used for the aircraft states are $\alpha = 1$ deg and $q = 2$ deg/sec. The adaptation parameters are initialized at zero, and the sigma modification is turned off. Generally, low adaptation rates reduce the adaptive contribution to the control signal.

 A critical point in the adaptation rate parameter space is the minimum value that has an influence on the aircraft response.

From that point, the trend in response due to increases in κ are studied. Simulation results exploring these effects are summarized in Fig. 6.2 and Fig. 6.3

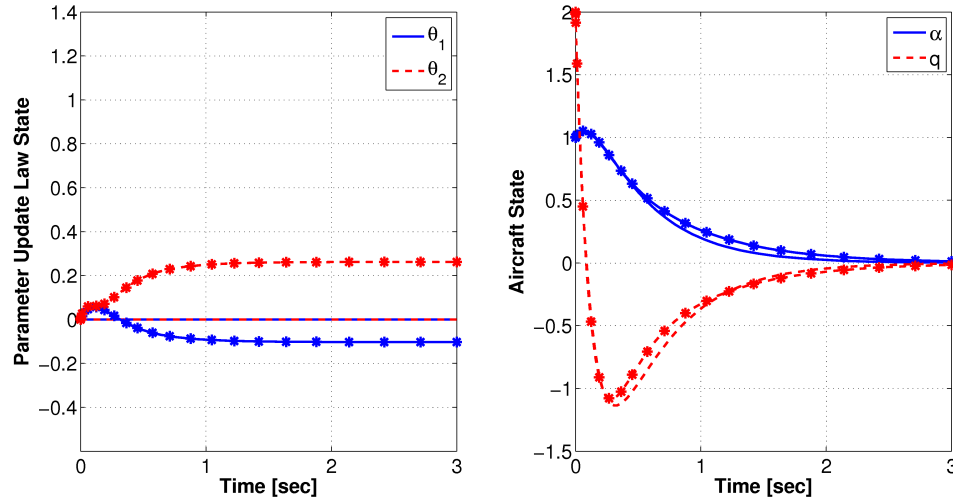


Figure 6.2: Finding minimum influential adaptation rate: $\kappa = [0, 0.5]$.

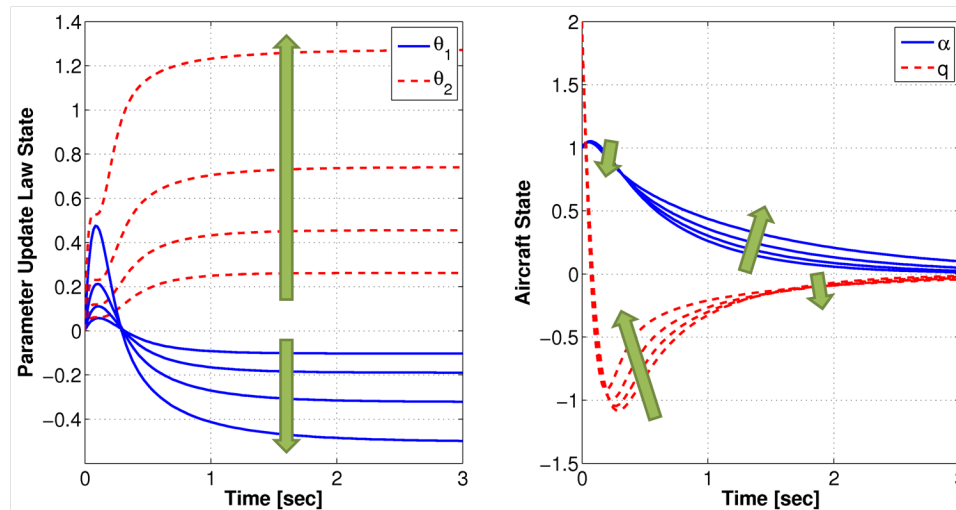


Figure 6.3: Trend in response due to increasing adaptation rate: $\kappa = [0.5, 1, 2, 5]$.



The results in Fig. 6.2 roughly identify the minimum value of κ for which the adaptive law has a noticeable effect on the aircraft dynamics. There are two simulation results in Fig. 6.2, one for $\kappa = 0$ and one for $\kappa = 0.5$. The $\kappa = 0.5$ results are highlighted with markers to indicate the change in response. The adaptation parameter response is shown on the left. For $\kappa = 0$, there is no response in the adaptation parameters since the adaptive law is not active. However, when $\kappa = 0.5$, the parameters react and level to non-zero steady state. Recall that for these simulations, sigma modification is turned off. Hence, the adaptation parameters do not converge near the origin. Sigma modification is turned off to isolate the effects due to changes in the adaptation rate.

The aircraft state response is shown on the right. The response deviates slightly by changing $\kappa = 0$ to $\kappa = 0.5$. Thus, in terms of the aircraft dynamics, $\kappa = 0.5$ approximates the minimum influential rate in the adaptive law.

Higher adaptation rates are simulated and the results are shown in Fig. 6.3. The sequence $\kappa = [0.5, 1, 2, 5]$ is used to illustrate trends in system response. Arrows indicate these trends with increasing adaptation rate. Larger values of κ cause more significant responses in the adaptation parameters, confirmed by the results in Fig. 6.3 on the left. The aircraft state response is shown on the right. Higher adaptation rate lowers the overshoot peak in the immediate transient. However, it also slightly increases the settling time. There is a trade-off between improving the immediate transient response versus the settling time.

The effect of extreme adaptation on the aircraft dynamics is also explored. It is important to have insight into the upper limit of desirable adaptation rates. Simulations are conducted for increasing κ at extreme values. The results are summarized in Fig. 6.4.

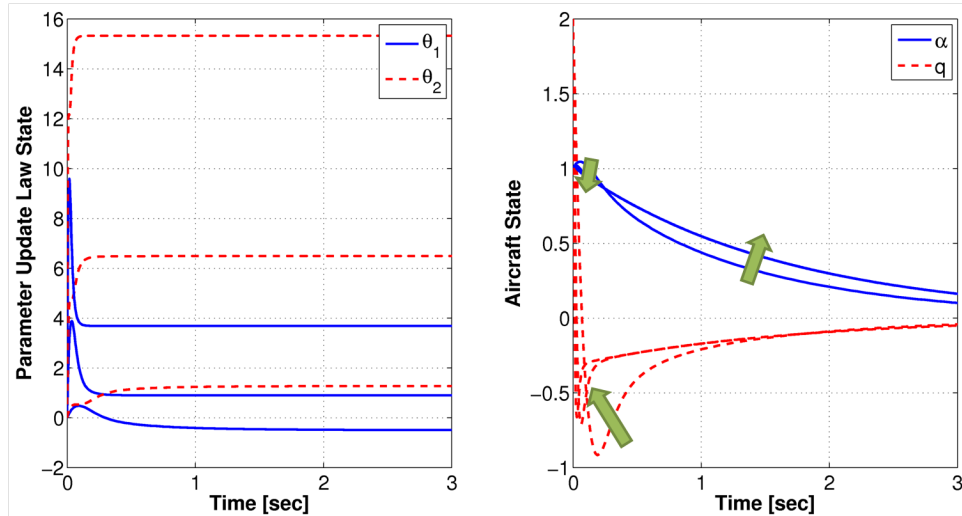


Figure 6.4: Trend in response due to increasing adaptation rate: $\kappa = [5, 100, 500]$.

The simulation results in Fig. 6.4 suggest that increasing the adaptation rate indefinitely provides diminishing returns with respect to the aircraft dynamics. The sequence $\kappa = [5, 100, 500]$ of adaptation rates are simulated. As κ increases, the adaptation parameters reach steady state more rapidly. The effect of increasing κ to extreme values is limited to altering the immediate transient in the aircraft response.

The settling time is not sensitive to changes in κ at extreme values. Increasing $\kappa = 100$ to $\kappa = 500$ has a negligible effect on the α response. Hence, only two curves appear to be plotted in Fig. 6.4. The response in q is affected by this change, but limited to a minimal reduction in overshoot. After 1.5 sec, the q response for $\kappa = 5$ is indistinguishable from $\kappa = 100$. It only takes 0.3 seconds for the $\kappa = 100$ and $\kappa = 500$ responses to converge. Thus, it is concluded that increasing the adaptation rate beyond 100 has minimal effects on the aircraft dynamics. A key observation is that the aircraft response is sensitive to varying adaptation rate on the interval $\kappa \in [0.5, 100]$.

The effect of varying adaptation rate on the robustness of the MRAC closed-loop system is explored by investigating time delay margins. The sigma modification term is constant at 1 for this analysis. The use of sigma modification is necessary in order to construct Lyapunov functions. An upper bound for the time delay margin is calculated using Monte Carlo simulations. The lower bound is calculated with SOS optimization. Time delay margin trends caused by variations in adaptation rate are summarized in Fig. 6.5.

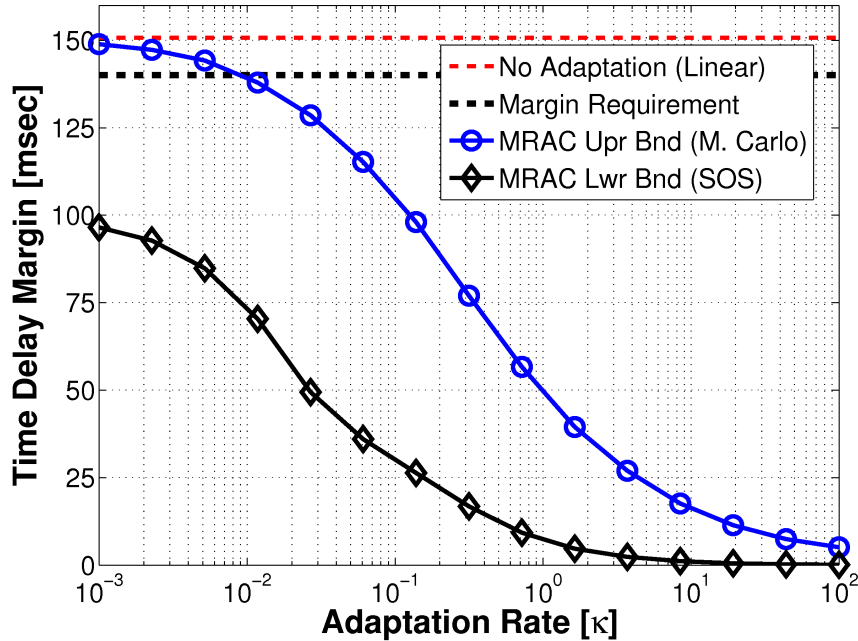


Figure 6.5: Time delay margin bounds as functions of adaptation rate.

The upper bound in Fig. 6.5 approaches the linear margin as adaptation rate decreases. Recall that the linear margin is found by turning off the adaptation. Upper

bound results confirm that decreasing κ leads to the convergence of the closed-loop system to the linear inner-loop. For $\kappa = 0.001$, the upper bound time delay margin converges to the linear margin. For higher adaptation gains, the upper bound decreases. For κ higher than 0.01, the minimum time delay margin requirement of 140 msec is no longer satisfied. At the same time, the smallest κ with influence on the aircraft dynamics is $\kappa = 0.5$. This result serves as a significant design constraint for the MRAC. The upper bound implies that it is impossible to design a controller that both benefits from adaptation and satisfies the robustness requirement.

Although the upper bound provides crucial insight, it alone is not sufficient to make claims about trends in the time delay margin. The upper bound is based on Monte Carlo simulations sampling random initial conditions and finding the lowest time delay causing resulting in trajectories. Generally, it is unclear how much sampling is needed to obtain an accurate upper bound. This is particularly the case for nonlinear systems, where potentially unforeseen nonlinear regions may exist in the state space. Thus, the upper bound may not accurately capture the trend in time delay margin. However, the existence of a lower bound with a similar trend increases confidence.

The lower bound in Fig. [6.5](#) is calculated with SOS optimization. It exhibits the same trend as the upper bound. The gap between the bounds is significant for low adaptation rates. However, the trend in the true time delay margin is obvious. Together, the upper and lower bounds show that the time delay margin is highly sensitive to changes in the adaptation rate when $\kappa \in [0.5, 100]$. This is a region of interest because the adaptive law has influence over the aircraft dynamics on this interval. Awareness of robustness sensitivity to changes in tuning parameters is crucial in control design. Although the MRAC does not satisfy the robustness requirements in the region of interest for adaptation rate, the relationship between adaptation rate and time delay margin is revealed. Such insight cannot be drawn without the existence of a calculated lower bound.

6.2 Sigma Modification

The parameter update law can also be tuned by varying sigma modification. Sigma modification is used in the MRAC architecture to guarantee the boundedness of states and to increase robustness. This parameter was held constant in the previous analysis. This section explores the reverse scenario by varying sigma modification for constant

adaptation rate. The adaptation rate is held constant at 1 for this analysis. This value belongs to the appropriate interval $\kappa \in [0.5, 100]$ discovered previously.

The main goal of using sigma modification is to increase robustness without sacrificing the benefits of adaptation. This is accomplished by ensuring that the adaptation parameters tend to the origin over time without disrupting their adaptive transient response. However, high values of sigma modification cause interference with the adaptive law and reduce its benefits. Extreme values can deactivate the adaptation completely. Simulations are used to provide insight into the appropriate range of sigma modification.

For the simulations, initial conditions in the aircraft state are $\alpha = 1$ deg and $q = 2$ deg/sec. These are the same conditions used in the previous section. The adaptation parameters are again initialized at the origin. The results in Fig. 6.6 identify the maximum allowable value of sigma modification with respect to the adaptive aircraft response.

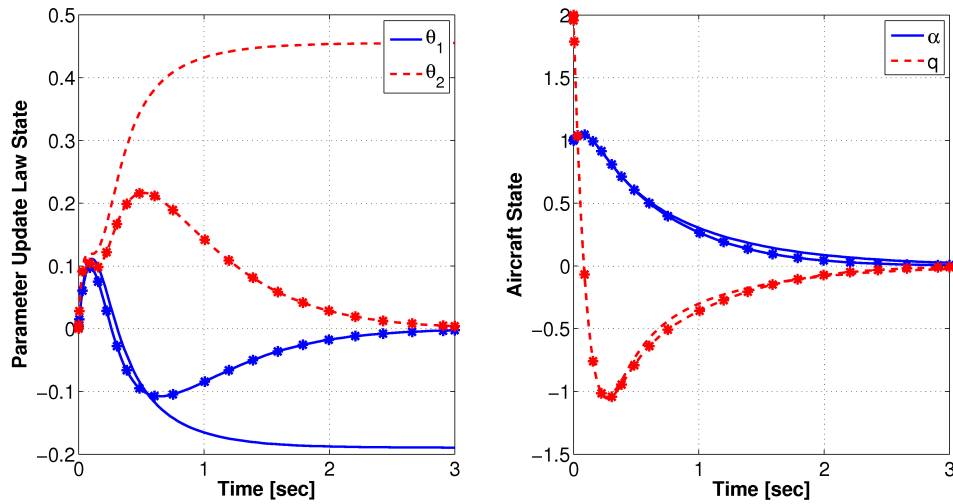


Figure 6.6: Finding maximum sigma modification value: $\sigma = [0, 2]$.

System response simulations for $\sigma = [0, 2]$ are shown in Fig. 6.6. The response for $\sigma = 2$ is distinguished with markers to highlight differences. Adaptation parameter response is shown on the left. For $\sigma = 0$, the adaptation parameters reach non-zero steady state. As desired, active sigma modification attracts them to the origin. The immediate transient is altered, but not significantly. The aircraft state response is shown on the right. For values less than 2, sigma modification has negligible

effects on the aircraft response. Beyond $\sigma = 2$, interference with the adaptive law becomes significant. Thus, $\sigma = 2$ represents the maximum allowable value of sigma modification for the closed-loop MRAC system. From a control design perspective, it is desirable to utilize as much sigma modification as possible to maximize system robustness.

In general, higher values of sigma modification result in more robustness to time delay. Extremely high values effectively turn off the parameter update law by holding the adaptation parameters near the origin. As such, the closed-loop system converges to the linear inner-loop. Recall that the time delay margin for this case is 151 msec. This is the expected time delay margin for extremely high values of sigma modification.

Time delay margin upper and lower bounds are calculated for the MRAC closed-loop system for varying sigma modification values. The upper bound is found with Monte Carlo simulations. The approach to the simulations is the same as in the previous section to find the upper bound. The lower bound is calculated using SOS optimization. The results in Fig. 6.7 summarize the effect of varying sigma modification on the lower and upper bounds of time delay margin.

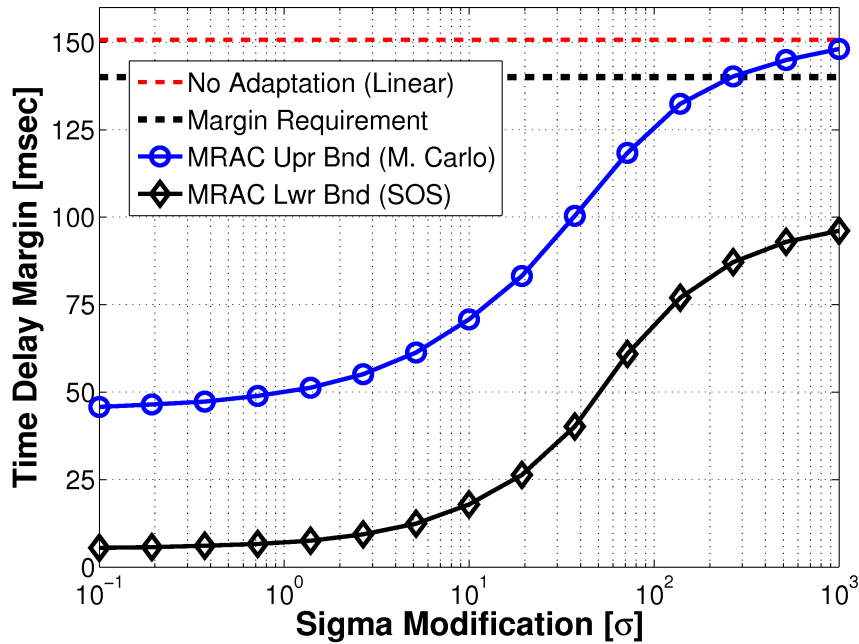


Figure 6.7: Time delay margin bounds as functions of sigma modification.

The upper bound in Fig. 6.7 suggests that robustness to time delay increases with

sigma modification. Further, it implies that the closed-loop system converges to the inner-loop for values above 1000. It is impossible to design an MRAC that meets the robustness requirement with sigma modification less than 300. However, selecting such a high value is not possible without reducing or eliminating the benefits of adaptation. Recall that the maximum beneficial value of sigma modification is $\sigma = 2$.

The lower bound results Fig. 6.7 exhibit a similar increasing trend as the upper bound. There is a constant 40 msec gap between the bounds as sigma modification varies. For values of sigma modification below 1, the lower bound is constant at 5 msec. The bound shows a steep increasing trend for values between 10 and 100, and levels out beyond 1000 at around 100 msec. The lower bound is not able to show that the minimum time delay margin robustness requirement is met for any value of sigma modification. However, it provides evidence that sigma modification cannot increase robustness without sacrificing performance in the adaptation.

Although the lower bound appears to be conservative, the bounds in Fig. 6.7 provide significant insight into the qualitative trend of the true time delay margin. The bounds imply that the time delay margin is constant for very low and very high values of sigma modification. They also indicate the range of values for which the time delay margin is most sensitive to changes in sigma modification. Knowledge of such sensitivities is crucial in control design. This type of insight cannot be drawn from the upper bound alone since it does not provide any analytically rigorous results. However, in conjunction with a guaranteed lower bound, the qualitative trends can be interpreted with more confidence.

6.3 Aircraft Model Uncertainty

The use of adaptive control is motivated by the need to account for uncertainty in the aircraft model without sacrificing performance. The goal of the MRAC is to ensure nominal aircraft performance in the presence of variations in the system dynamics. Uncertainty is represented through the λ scaling parameters in the state matrix of the aircraft model. Each parameter varies on the interval $[0.25, 1.75]$ to encompass 75% uncertainty. A family of inner-loop transfer functions from elevator input to angle-of-attack output is calculated for this interval. Fig. 6.8 shows the frequency response of this family of transfer functions to illustrate the effect of uncertainty on the aircraft dynamics.

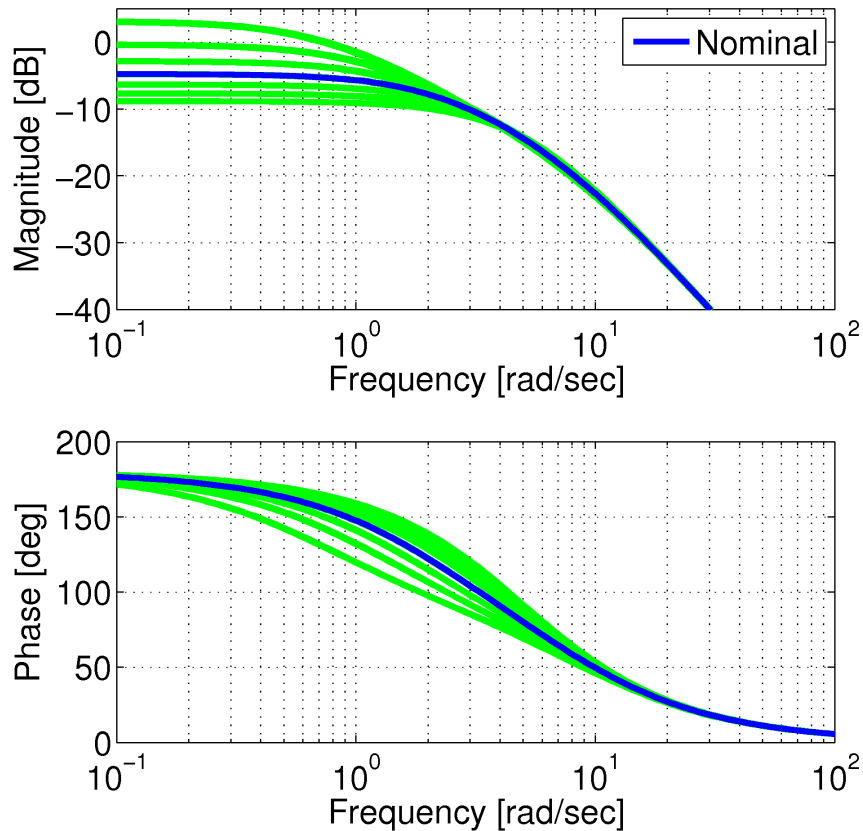


Figure 6.8: Bode plot illustrating aircraft model uncertainty.



The results in Fig. 6.8 suggest that uncertainty in the aircraft model is limited to changes in the low frequency characteristics of the inner-loop system. The nominal model is highlighted with the darker line on the plot. Deviations from the nominal model increase and decrease the DC gain of the system. The bandwidth of the system varies, but this fluctuation does not affect the high frequency asymptote. Hence, the roll-off of the system is not affected. This implies that the modes of the system do not vary independently due to uncertainty.

Another way to gain insight into the uncertainty is to explore the location of the inner-loop poles. Direct analysis of pole location can indicate movement towards the imaginary axis. It can also indicate the transition from real poles to complex poles. Fig. 6.9 shows the loci of the inner-loop poles by sweeping over possible combinations of the uncertainty parameters.

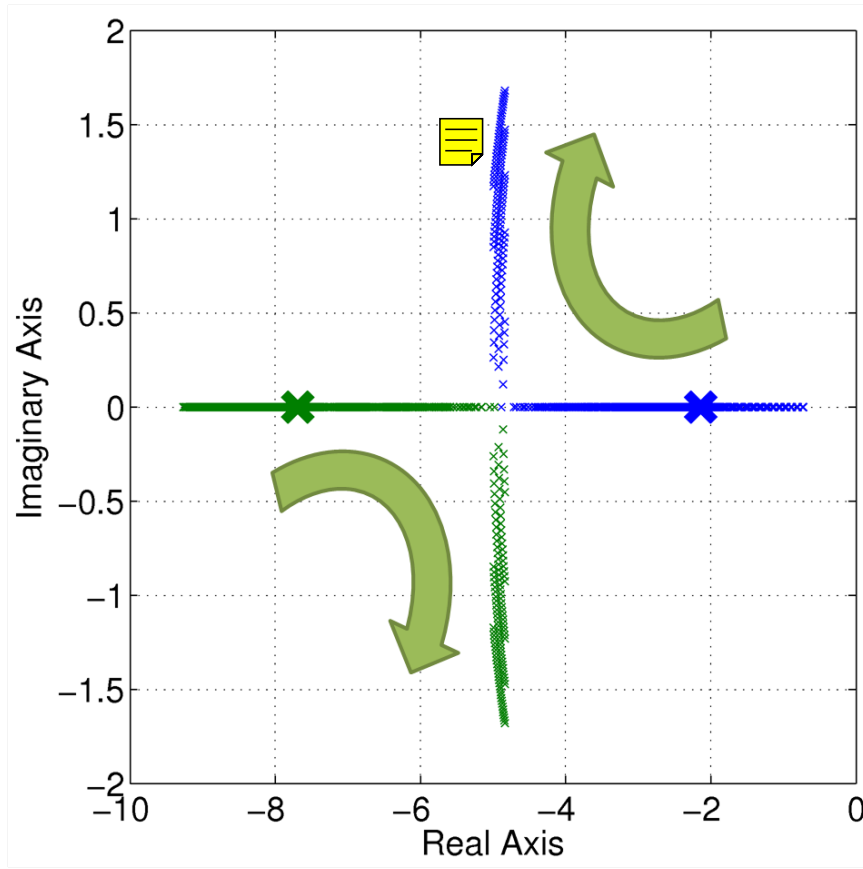


Figure 6.9: Root locus due to aircraft model uncertainty.

The results in Fig. 6.9 illustrate the effects of uncertainty on the modes of the inner-loop system. The nominal model's poles are highlighted by the large symbols. Each λ parameter is varied across the interval $[0.25, 1.75]$ on a grid in steps of 0.05. Analysis of pole movement suggests that the inner-loop dynamics are more sensitive to changes in λ_α than in λ_q . Arrows in Fig. 6.9 indicate the general trend due to increasing λ_α . Increasing λ_α decreases the damping ratio in the system. However, a decrease in the same parameter moves one of the poles closer to the imaginary axis.

The frequency response in Fig. 6.8 and the root locus in Fig. 6.9 suggest that variations in the inner-loop due to 75% uncertainty are mild. In particular, the system remains stable for all possible choices of uncertainty. The smallest perturbation causing instability in the inner-loop is $\lambda_\alpha = \lambda_q = -0.26$. This case represents 126% parametric uncertainty, which is well above the range considered in this analysis.



Time delay margins are calculated in the presence of 100% uncertainty in the aircraft model to gain insight into the effects on robustness. The MRAC is designed with

sigma modification and adaptation rates in the appropriate parameter ranges found in the previous sections. An adaptation rate of 1 is selected for the adaptive law. This value is in the range of desirable adaptive dynamics. A sigma modification value of 1 is used, supplying maximum robustness without sacrificing performance in adaptation. Upper and lower bounds on the time delay margin are calculated with Monte Carlo simulations and SOS optimization, respectively. The upper and lower bound results are summarized in Fig. 6.10.

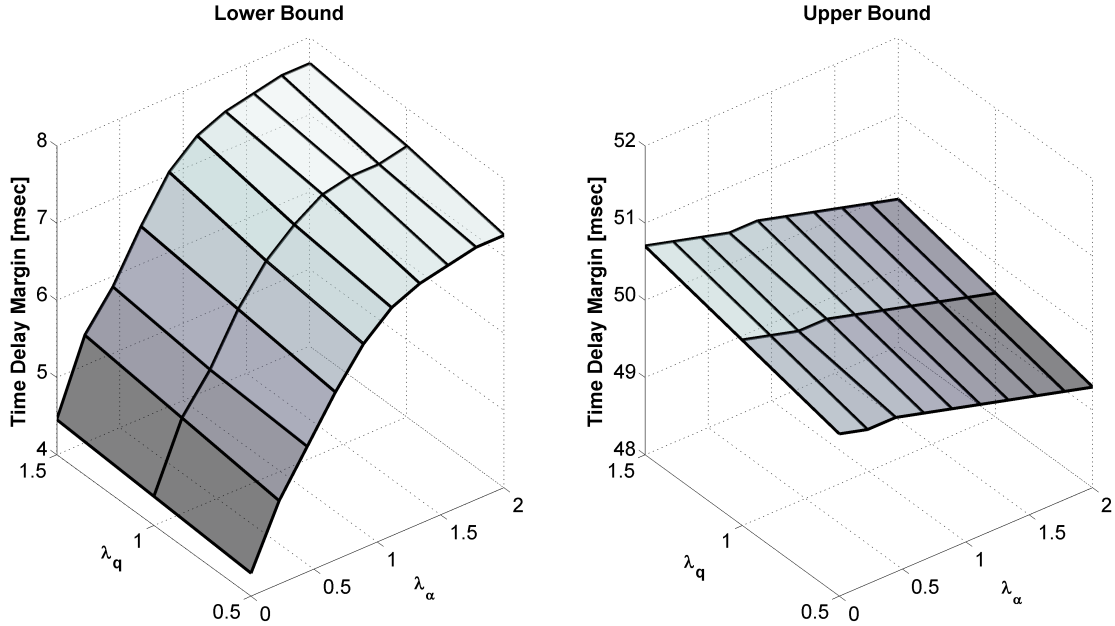


Figure 6.10: Time delay margin bounds as functions of aircraft model uncertainty.

The upper bound is shown in Fig. 6.10 on the right. It confirms that the system robustness is not equally sensitive to variations in the two uncertainty parameters. The system is less sensitive to fluctuations in λ_q than in λ_α . Hence, for computing the lower bound, a less refined grid is used in the λ_q direction in the interest of reducing computation time. The grid on λ_q is coarse, and fine on λ_α .

The lower bound is shown on the left in Fig. 6.10. Time delay margin increases with the uncertainty parameter λ_α . As predicted, the results are not sensitive to changes in λ_q . The upper bound on the time delay margin is relatively constant at around 50 msec. The SOS optimization is less effective than in previous results at capturing the trend in time delay margin. However, it is still able to guarantee a robustness margin bounded away from zero. Improvement in the calculation of the lower bound

is necessary.

Without the SOS optimization nonlinear analysis tool, the calculation of meaningful lower bounds on time delay margin is not possible. Other tools for this type of nonlinear analysis do not exist. Hence, the SOS results in the previous analyses are significant. The lower bounds are conservative and improvements can be made. The key point is, however, that robustness analysis is not possible without both an upper bound and a lower bound. Hence, the SOS approach is a notable step towards rigorous nonlinear analysis.

6.4 Limitations

The single greatest limitation of the SOS optimization approach for calculating time delay margin is the shortage of memory and computation time. Roughly, the bisection done for each data point takes 20 minutes on a quad-core Intel processor. Due to the structure of the Lyapunov function, the state order of the MRAC closed-loop system is tripled. Two extra sets of state variables are required to handle time delay, resulting in a total of 12 states. Thus, the Lyapunov function in the SOS optimization is limited to being a second order polynomial. The computational load grows with the state order of the model. As such, computers run out of memory when attempting to solve time delay MRAC problems with cubic Lyapunov functions. Simpler examples have shown less conservative results for higher order Lyapunov functions [19]. With the current approach to SOS optimization, this is a fundamental limitation.

The assumptions made in the derivation of the SOS conditions are also limiting. Most obviously, the dynamics must be polynomial. If the dynamics of a system are not polynomial, they must be approximated as such. The model is also assumed to be autonomous. The consideration of an input signal is not possible. Hence, stability guarantees can only be made for the internal dynamics of a system.

Chapter 7

Conclusion

Adaptive control algorithms have the potential to improve performance and robustness in aerospace systems. However, there is a lack of tools available to rigorously analyze the robustness of these systems. This thesis uses polynomial optimization tools to show the suitability of such analysis in the verification of adaptive control systems. The robustness of a model reference adaptive controller for a short period aircraft model is examined.

The robustness metric calculated for the adaptive controller is the time delay margin. Time delay margin guarantees the amount of time delay a system can tolerate before losing stability. The analysis provides insight into the effects of varying adaptation rate and sigma modification, both tuning parameters in the adaptive controller. The effects of uncertainty are also explored. Future work includes refining the theoretical approach with more complex algorithms known to provide even less conservative results.

The key contribution of this thesis is the application of a nonlinear analysis tool for evaluating the robustness of a short period aircraft model with model reference adaptive control. This tool was previously applied to evaluate the robustness of trivial polynomial systems. This thesis applies the nonlinear approach to a relevant adaptive flight control problem. The goal of this research is not to make claims about the validity of any particular adaptive control architecture. Rather, the focus is on using analysis tools that can be applied generally to polynomial adaptive controllers. Several key modeling simplifications are made which lead to biases in the results. In

spite of these biases, the robustness analysis results in this thesis are significant in light of the sparsely populated realm of nonlinear analysis tools.

Bibliography

- [1] Parrilo, P., *Structured Semidefinite Programs and Semialgebraic Geometry Methods in Robustness and Optimization*, Ph.D. thesis, California Institute of Technology, 2000.
- [2] Lasserre, J., “Global Optimization with Polynomials and the Problem of Moments,” *SIAM Journal on Optimization*, Vol. 11, No. 3, 2001, pp. 796–817.
- [3] Parrilo, P., “Semidefinite programming relaxations for semialgebraic problems,” *Mathematical Programming Ser. B*, 2003.
- [4] Tibken, B., “Estimation of the domain of attraction for polynomial systems via LMIs,” *Proceedings of the IEEE Conference on Decision and Control*, 2000, pp. 3860–3864.
- [5] Hachicho, O. and Tibken, B., “Estimating domains of attraction of a class of nonlinear dynamical systems with LMI methods based on the theory of moments,” *Proceedings of the IEEE Conference on Decision and Control*, 2002, pp. 3150–3155.
- [6] Jarvis-Wloszek, Z., *Lyapunov Based Analysis and Controller Synthesis for Polynomial Systems using Sum-of-Squares Optimization*, Ph.D. thesis, University of California, Berkeley, 2003.
- [7] Jarvis-Wloszek, Z., Feeley, R., Tan, W., Sun, K., and Packard, A., “Some Controls Applications of Sum of Squares Programming,” *Proceedings of the 42nd IEEE Conference on Decision and Control*, Vol. 5, 2003, pp. 4676–4681.
- [8] Papachristodoulou, A., *Scalable analysis of nonlinear systems using convex optimization*, Ph.D. thesis, California Institute of Technology, 2005.

- [9] Jarvis-Wloszek, Z., Feeley, R., Tan, W., Sun, K., and Packard, A., *Positive Polynomials in Control*, Vol. 312 of *Lecture Notes in Control and Information Sciences*, chap. Controls Applications of Sum of Squares Programming, Springer-Verlag, 2005, pp. 3–22.
- [10] Chesi, G., Garulli, A., Tesi, A., and Vicino, A., “LMI-based computation of optimal quadratic Lyapunov functions for odd polynomial systems,” *International Journal of Robust and Nonlinear Control*, Vol. 15, 2005, pp. 35–49.
- [11] Prajna, S., *Optimization-Based Methods for Nonlinear and Hybrid Systems Verification*, Ph.D. thesis, California Institute of Technology, 2005.
- [12] Tan, W., Packard, A., and Wheeler, T., “Local gain analysis of nonlinear systems,” *Proceedings of the American Control Conference*, pp. 92–96.
- [13] Tan, W., *Nonlinear Control Analysis and Synthesis using Sum-of-Squares Programming*, Ph.D. thesis, University of California, Berkeley, 2006.
- [14] Tibken, B. and Fan, Y., “Computing the domain of attraction for polynomial systems via BMI optimization methods,” *Proceedings of the American Control Conference*, 2006, pp. 117–122.
- [15] Tan, W., Topcu, U., Seiler, P., Balas, G., and Packard, A., “Simulation-aided Reachability and Local Gain Analysis for Nonlinear Dynamical Systems,” *Proceedings of the IEEE Conference on Decision and Control*, 2008, pp. 4097–4102.
- [16] Topcu, U., Packard, A., and Seiler, P., “Local stability analysis using simulations and sum-of-squares programming,” *Automatica*, Vol. 44, No. 10, 2008, pp. 2669–2675.
- [17] Topcu, U., *Quantitative Local Analysis of Nonlinear Systems*, Ph.D. thesis, University of California, Berkeley, 2008.
- [18] Topcu, U. and Packard, A., “Linearized analysis versus optimization-based nonlinear analysis for nonlinear systems,” *Proceedings of the American Control Conference*, 2009.
- [19] Papachristodoulou, A., “Analysis of Nonlinear Time-Delay Systems using Sum of Squares Decomposition,” *Proceedings of the American Control Conference*, 2004, pp. 4153–4158.

- [20] Papachristodoulou, A., Peet, M., and Lall, S., “Analysis of Polynomial Systems With Time Delays via Sum of Squares Decomposition,” *IEEE Transactions on Automatic Control*, Vol. 54, No. 5, 2009.
- [21] Prajna, S., Papachristodoulou, A., Seiler, P., and Parrilo, P. A., *SOSTOOLS: Sum of squares optimization toolbox for MATLAB*, 2004.
- [22] Lofberg, J., “YALMIP : A Toolbox for Modeling and Optimization in MATLAB,” *Proceedings of the CACSD Conference*, Taipei, Taiwan, 2004.
- [23] Balas, G., Packard, A., Seiler, P., and Topcu, U., “Robustness Analysis of Non-linear Systems,” <http://aem.umn.edu/~AerospaceControl/>.
- [24] Seiler, P., Balas, G., Packard, A., and Topcu, U., “Analytical Validation Tools for Safety Critical Systems,” *AIAA Infotech@Aerospace Conference*, No. AIAA 2009-1991, 2009.
- [25] Cook, M., *Flight Dynamics Principles*, Elsevier Ltd., 2007.
- [26] Annaswamy, A., Jang, J., and Lavretsky, E., “Stability margins for adaptive controllers in the presence of time delay,” *AIAA Guidance, Navigation, and Control Conference*, No. AIAA 2008-6659, 2008.
- [27] Skogestad, S. and Postlethwaite, I., *Multivariable Feedback Control*, John Wiley and Sons Ltd., 2007.
- [28] Ioannou, P. and Sun, J., *Robust Adaptive Control*, Prentice Hall, 1995.
- [29] Narendra, K. and Annaswamy, A., *Stable Adaptive Systems*, Prentice Hall, 1989.
- [30] Sturm, J., “SeDuMi version 1.05,” <http://fewcal.kub.nl/sturm/software/sedumi.html>, 2001.
- [31] Sturm, J., “Using SeDuMi 1.02, a MATLAB toolbox for optimization over symmetric cones,” *Optimization Methods and Software*, 1999, pp. 625–653.
- [32] Gatermann, K. and Parrilo, P., “Symmetry groups, semidefinite programs, and sums of squares,” *Journal of Pure and Applied Algebra*, Vol. 192, 2004, pp. 95–128.
- [33] Ogata, K., *Modern Control Engineering*, Prentice Hall, 4th ed., 2002.